Analysis of nonlocal effective permittivity and permeability in symmetric metal–dielectric multilayer metamaterials

2016 J. Opt. 18 065101

(http://iopscience.iop.org/2040-8986/18/6/065101)

IOP Publishing Journal of Optics
J. Opt. 18 (2016) 065101 (11pp) doi:10.1088/2040-8978/18/6/065101

Analysis of nonlocal effective permittivity and permeability in symmetric metal–dielectric multilayer metamaterials

Lei Sun, Xiaodong Yang[1] and Jie Gao[1]

Department of Mechanical and Aerospace Engineering Missouri University of Science and Technology Rolla, Missouri 65409, USA

E-mail: yangxia@mst.edu and gaojie@mst.edu

Received 20 January 2016, revised 26 February 2016
Accepted for publication 3 March 2016
Published 13 April 2016

Abstract

A generalized nonlocal effective medium theory is derived based on the transfer-matrix method to determine the nonlocal effective permittivity and permeability for the symmetric and periodic metal–dielectric multilayer metamaterials, with respect to both transverse-electric and transverse-magnetic polarized light at arbitrary angle of incidence. The nonlocal effective permittivity and permeability tensors are analyzed in detail as functions of the wavelength, the angle of incidence, and the multilayer period. Our generalized nonlocal effective medium theory in consideration of both permittivity and permeability can accurately predict the dispersion relation, the transmission and reflection spectra, and the optical field distributions of symmetric metal–dielectric multilayer stacks with either subwavelength or wavelength-scale period of the unit cell.

Keywords: metamaterials, dispersion, optical nonlocality, effective medium

(Some figures may appear in colour only in the online journal)

1. Introduction

Recently metal–dielectric multilayer metamaterials have been widely explored due to their anomalous electromagnetic properties in optical frequencies. Metal–dielectric multilayer metamaterials with hyperbolic dispersion have been used to realize many unique applications [1], such as negative refraction [2–4], deep subwavelength imaging [5–7], anomalous indefinite cavity [8], photonic density of states enhancement [9, 10], thermal emission design [11], and spontaneous emission engineering [12–14]. By tuning the metallic filling ratio of metal–dielectric multilayer stacks, epsilon-near-zero (ENZ) metamaterials can be constructed for the realization of radiation wavefront tailoring [15], displacement current insulation [16, 17], optical nonlinearity enhancement [18], and invisible cloaking [19, 20]. The optical properties of metal–dielectric multilayer stacks can be simply described by the local effective medium theory (EMT), when the multilayer period is much smaller than the optical wavelength. In fact, due to the dramatically different electromagnetic properties of the metal layer and the dielectric layer, the variation of the electromagnetic field on the scale of one multilayer period will generate strong spatial dispersion, which will lead to optical nonlocality [21] not considered in the local EMT. Recently, in order to take into account the optical nonlocality in metal–dielectric multilayer stacks, several different nonlocal EMT models have been derived, such as the dispersion relation approximation [22–24] and the electromagnetic field averaging algorithm [25–27]. However, these models only consider the nonlocal effective permittivity as functions of frequency and wave vector, but assume unity permeability. Therefore, the optical properties of metal–dielectric multilayer stacks cannot be completely predicted by these models, especially when the multilayer period is far away from the deep-subwavelength scale.

According to Herpin's theorem, any dielectric multilayer stack is equivalent to a two-film combination [28], while a symmetric dielectric multilayer stack is equivalent to a single film with an effective refractive index [29–31] based on the transfer-matrix method [32]. Therefore, in this work, a generalized nonlocal EMT in consideration of both nonlocal

[1] Authors to whom any correspondence should be addressed.

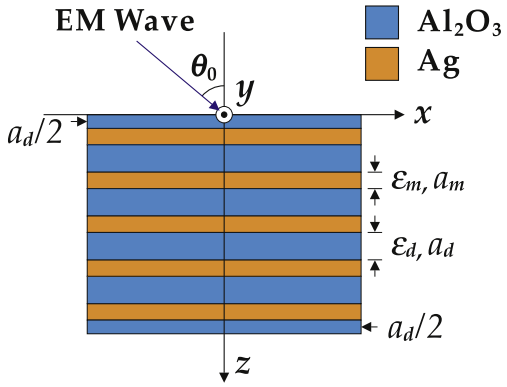

Figure 1. Schematic of the symmetric and periodic Ag-Al_2O_3 multilayer stack with respect to the AOI θ_0 in free space.

effective permittivity and permeability is derived for the symmetric metal–dielectric multilayer stack with respect to both transverse-electric (TE) and transverse-magnetic (TM) polarized light with arbitrary angle of incidence (AOI). The nonlocal effective permittivity and permeability tensors will be obtained through the transfer-matrix method in order to fully describe the variation of the electromagnetic field across the metal–dielectric multilayers with respect to both frequency and wave vector. Compared with the local EMT parameters, the nonlocal effective permittivity and permeability tensors are analyzed in detail as functions of the wavelength, the angle of incidence, as well as the multilayer period. It is shown that the generalized nonlocal EMT will converge into the local EMT as the multilayer period approaches zero. In general, in contrast to the local EMT, the generalized nonlocal EMT can fully characterize the optical properties of the symmetric metal–dielectric multilayer stacks with either subwavelength or wavelength-scale period of the unit cell, and accurately predict the band structures, the iso-frequency contours (IFCs), the transmission and reflection spectra, as well as the optical field distributions.

2. Development of generalized nonlocal effective medium theory

Figure 1(a) illustrates the symmetric and periodic metal–dielectric multilayer stack composed of five-pair (with $N = 5$) symmetric unit cells. Each unit cell contains a silver (Ag) layer with the thickness of a_m sandwiched between two sapphire (Al_2O_3) layers with the thickness of $a_d/2$, under the illumination of the incident light propagating in the x-z plane with an arbitrary AOI θ_0 in free space. The thickness of one unit cell is $a = a_m + a_d$, while the total thickness of the multilayer stack is $a_{\text{tot}} = Na$. The electric permittivities of the Ag layer and the Al_2O_3 layer are denoted as ε_m and ε_d, respectively. The magnetic permeabilities of the Ag layer and the Al_2O_3 layer are denoted as μ_m and μ_d, which are equal to unity. In general, the symmetric Ag-Al_2O_3 multilayer stack can be regarded as a bulk of homogenous and anisotropic effective medium characterized by a set of effective parameters, that is, a diagonal permittivity tensor and a diagonal permeability tensor. According to the local EMT, the local effective permittivity tensor reads $\bar{\varepsilon}^{\text{loc}} = \text{diag}(\varepsilon_x^{\text{loc}}, \varepsilon_y^{\text{loc}}, \varepsilon_z^{\text{loc}})$ with $\varepsilon_x^{\text{loc}} = \varepsilon_y^{\text{loc}} = (\varepsilon_m a_m + \varepsilon_d a_d)/(a_m + a_d)$ and $\varepsilon_z^{\text{loc}} = \varepsilon_m \varepsilon_d (a_m + a_d)/(\varepsilon_m a_d + \varepsilon_d a_m)$, which only depend on frequency. Meanwhile, the local effective permeability tensor is always equal to unity. In fact, previous studies have shown that metal–dielectric multilayer stacks possess strong spatial dispersion caused by optical nonlocality, which cannot be characterized by the local EMT. Furthermore, the previously proposed nonlocal EMT models only consider the nonlocal effective permittivity tensor as a function of both frequency and wave vector, but the nonlocal effective permeability tensor is still treated as unity so that the optical properties of the metal–dielectric multilayer stacks cannot completely predicted yet.

In order to take into account the optical nonlocality accurately, a generalized nonlocal EMT is derived through the transfer-matrix method, and both the nonlocal effective permittivity and permeability tensors are introduced as functions of frequency and wave vector. In accordance with the boundary conditions, the tangential components of the electromagnetic field should be continuous across all interfaces of the Ag-Al_2O_3 multilayer stack. Then the transfer matrix for the multilayer stack composed of five-pair unit cells is described as

$$\boldsymbol{M}_{\text{stack}} = \boldsymbol{M}_{\text{cell}}^5 = (\boldsymbol{M}_{d/2} \cdot \boldsymbol{M}_m \cdot \boldsymbol{M}_{d/2})^5, \tag{1}$$

in which

$$\boldsymbol{M}_m = \begin{bmatrix} \cos(\sqrt{\varepsilon_m \mu_m} k_0 a_m \cos\theta_m) & -\mathrm{i}\sin(\sqrt{\varepsilon_m \mu_m} k_0 a_m \cos\theta_m)/\eta_m \\ -\mathrm{i}\sin(\sqrt{\varepsilon_m \mu_m} k_0 a_m \cos\theta_m)\eta_m & \cos(\sqrt{\varepsilon_m \mu_m} k_0 a_m \cos\theta_m) \end{bmatrix} \tag{2}$$

for the Ag layer, and

$$\boldsymbol{M}_{d/2} = \begin{bmatrix} \cos(\sqrt{\varepsilon_d \mu_d} k_0 \cdot a_d/2 \cdot \cos\theta_d) & -\mathrm{i}\sin(\sqrt{\varepsilon_d \mu_d} k_0 \cdot a_d/2 \cdot \cos\theta_d)/\eta_d \\ -\mathrm{i}\sin(\sqrt{\varepsilon_d \mu_d} k_0 \cdot a_d/2 \cdot \cos\theta_d)\eta_d & \cos(\sqrt{\varepsilon_d \mu_d} k_0 \cdot a_d/2 \cdot \cos\theta_d) \end{bmatrix} \tag{3}$$

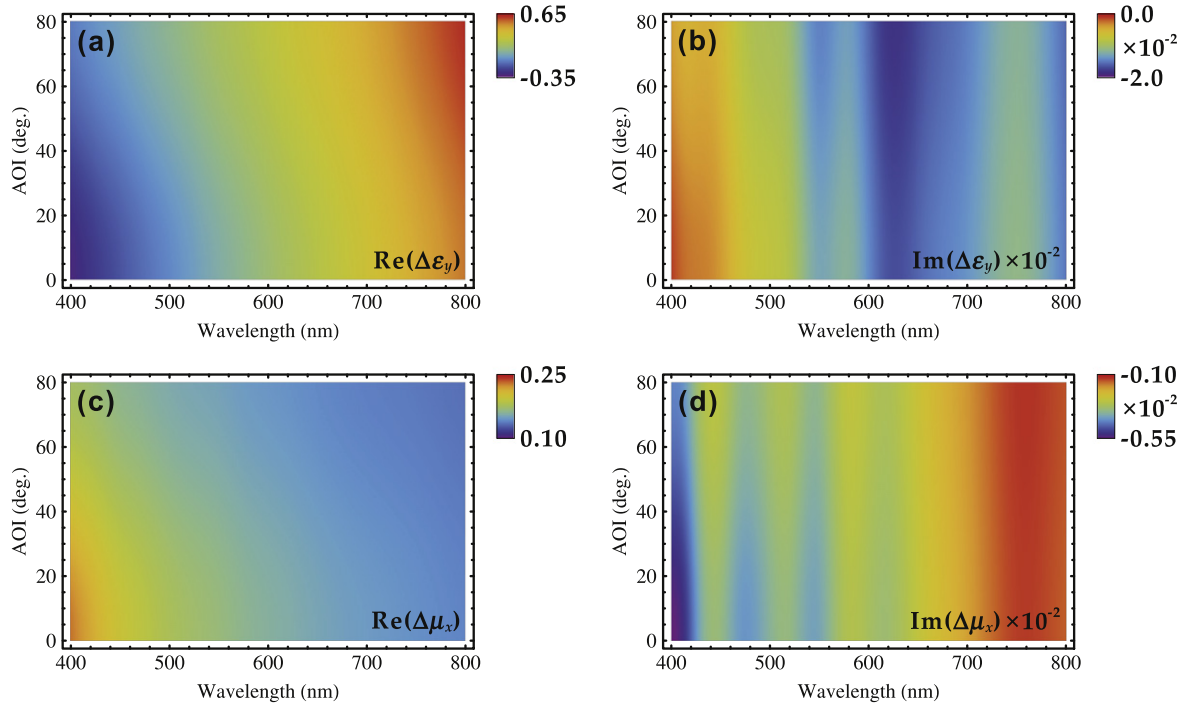

Figure 2. (a) The real part and (b) the imaginary part of $\Delta\varepsilon_y = \varepsilon_y - \varepsilon_y^{\mathrm{loc}}$, as well as (c) the real part and (d) the imaginary part of $\Delta\mu_x = \mu_x - \mu_x^{\mathrm{loc}}$, with respect to the variations of wavelength and AOI for TE polarized light.

for the Al_2O_3 half layer. The parameter η_i reads $\eta_i = \sqrt{\varepsilon_i\mu_i}\cos\theta_i$ for TE polarized light and $\eta_i = \sqrt{\mu_i/\varepsilon_i}\cos\theta_i$ for TM polarized light. The angle of refraction θ_i is determined by the AOI θ_0 as $k_x = k_0\sin\theta_0 = \sqrt{\varepsilon_i\mu_i}k_0\sin\theta_i$ with $i = m$ and d for the Ag layer and Al_2O_3 layer, respectively. Considering the symmetric and periodic properties of the Ag-Al_2O_3 multilayer stack, the connections between the transfer matrix for the stack $\boldsymbol{M}_{\mathrm{stack}}$ and the transfer matrix for the unit cell $\boldsymbol{M}_{\mathrm{cell}}$ can be studied. According to equations (1)–(3), $\boldsymbol{M}_{\mathrm{cell}}$ can be expressed as

$$\boldsymbol{M}_{\mathrm{cell}} = \begin{bmatrix} \cos(k_z a) & -\mathrm{i}\sin(k_z a)/\eta_e \\ -\mathrm{i}\sin(k_z a)\eta_e & \cos(k_z a) \end{bmatrix}, \tag{4}$$

in terms of the dispersion relation of the unit cell

$$\cos(k_z a) = \cos\varphi_d\cos\varphi_m - \frac{1}{2}\left(\frac{\eta_d}{\eta_m} + \frac{\eta_m}{\eta_d}\right)\sin\varphi_d\sin\varphi_m \tag{5}$$

and the parameter

$$\eta_e = \sqrt{\frac{\eta_d^2\left[2\eta_d\eta_m\sin\varphi_d\cos\varphi_m + (-\eta_d^2 + \eta_m^2 + (\eta_d^2 + \eta_m^2)\cos\varphi_d)\sin\varphi_m\right]}{2\eta_d\eta_m\sin\varphi_d\cos\varphi_m + (\eta_d^2 - \eta_m^2 + (\eta_d^2 + \eta_m^2)\cos\varphi_d)\sin\varphi_m}} \tag{6}$$

with $\varphi_d = \sqrt{\varepsilon_d\mu_d}k_0 a_d\cos\theta_d$ and $\varphi_m = \sqrt{\varepsilon_m\mu_m}k_0 a_m\cos\theta_m$. On the other hand, $\boldsymbol{M}_{\mathrm{stack}}$ with N unit cell is determined as

$$\boldsymbol{M}_{\mathrm{stack}} = \begin{bmatrix} \cos(k_z\cdot Na) & -\mathrm{i}\sin(k_z\cdot Na)/\eta_e \\ -\mathrm{i}\sin(k_z\cdot Na)\eta_e & \cos(k_z\cdot Na) \end{bmatrix}, \tag{7}$$

based on the Chebyshev polynomials of the second kind. By comparing equations (4) and (7), it is indicated that the electromagnetic field distribution in the Ag-Al_2O_3 multilayer stack can be fully described by that in the symmetric unit cell. This fact implies that the nonlocal effective parameters for the stack are independent of the number of the unit cell N. Therefore, only one symmetric unit cell will be considered in the determination of the nonlocal effective permittivity and permeability tensors.

The symmetric unit cell is considered as a homogenous and anisotropic effective medium including the optical nonlocality with the nonlocal effective permittivity and permeability tensors of $\bar{\varepsilon}_e = \mathrm{diag}(\varepsilon_x, \varepsilon_y, \varepsilon_z)$ and $\bar{\mu}_e = \mathrm{diag}(\mu_x, \mu_y, \mu_z)$. The transfer matrix for the unit cell regarded as a nonlocal effective medium is represented as

$$\boldsymbol{M}_{\mathrm{eff}} = \begin{bmatrix} \cos(k_z a) & -\mathrm{i}\sin(k_z a)/\eta_{\mathrm{eff}} \\ -\mathrm{i}\sin(k_z a)\eta_{\mathrm{eff}} & \cos(k_z a) \end{bmatrix}, \tag{8}$$

where the parameter

$$\eta_{\mathrm{eff}} = \frac{k_z}{\mu_x k_0} \tag{9}$$

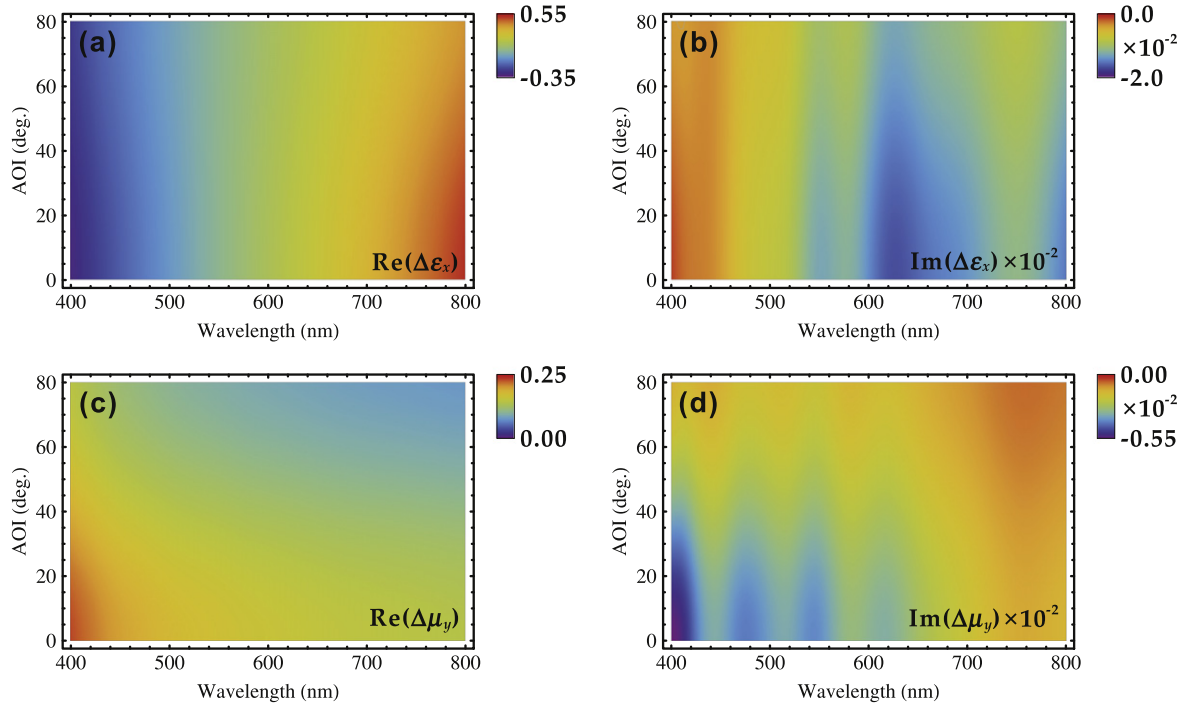

Figure 3. (a) The real part and (b) the imaginary part of $\Delta\varepsilon_x = \varepsilon_x - \varepsilon_x^{\mathrm{loc}}$, as well as (c) the real part and (d) the imaginary part of $\Delta\mu_y = \mu_y - \mu_y^{\mathrm{loc}}$, with respect to the variations of wavelength and AOI for TM polarized light.

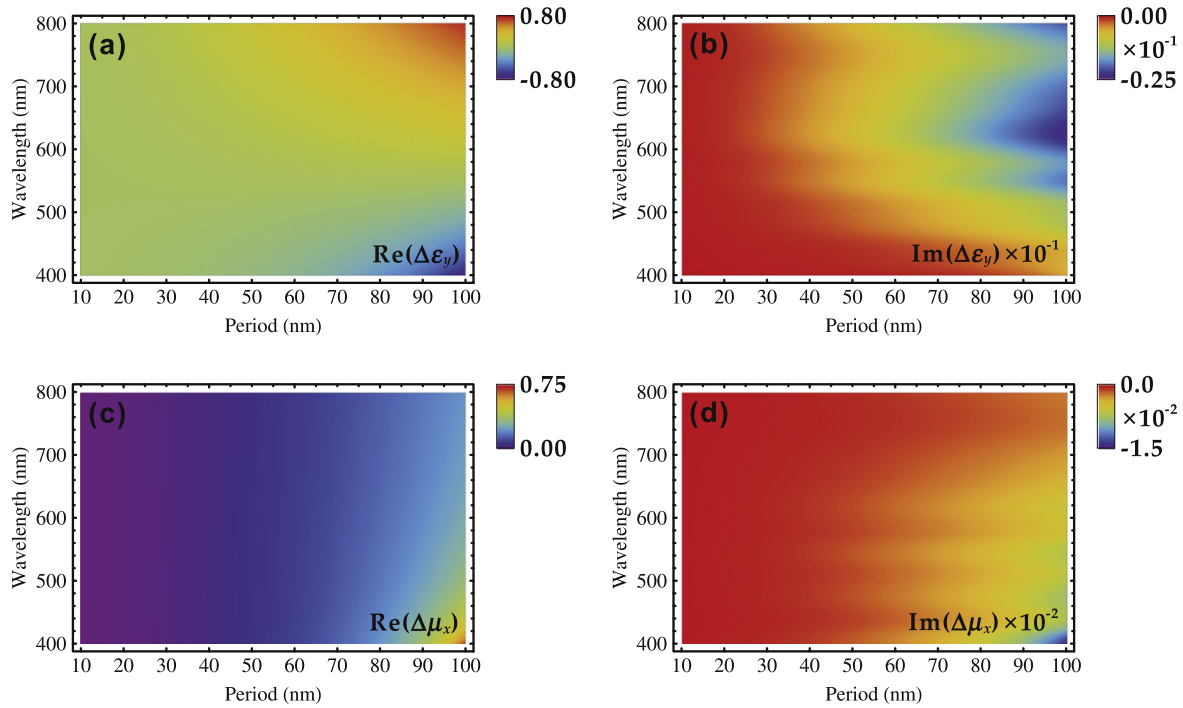

Figure 4. (a) The real part and (b) the imaginary part of $\Delta\varepsilon_y = \varepsilon_y - \varepsilon_y^{\mathrm{loc}}$, as well as (c) the real part and (d) the imaginary part of $\Delta\mu_x = \mu_x - \mu_x^{\mathrm{loc}}$, with respect to the variations of the period of the unit cell and wavelength for TEM mode at zero AOI.

for the TE polarized light, and

$$\eta_{\mathrm{eff}} = \frac{k_z}{\varepsilon_x k_0} \tag{10}$$

for the TM polarized light. Since the nonlocal effective medium should represent the unit cell, the relation of $\eta_{\mathrm{eff}} \equiv \eta_e$ should be satisfied for both TE and TM polarized light, according to equations (4) and (8). Meanwhile, the

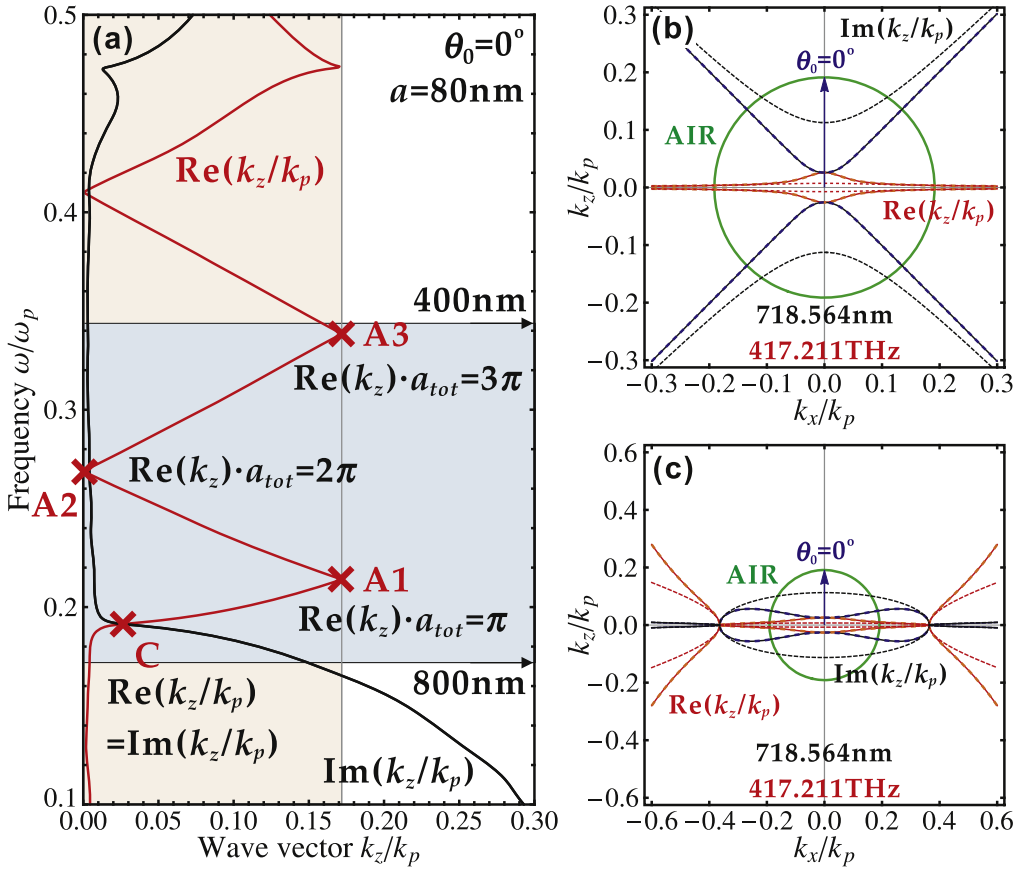

Figure 5. (a) The band structure of the Ag-Al_2O_3 multilayer stack with the period of unit cell $a = 80$ nm at zero AOI. The real part of the normalized wave vector k_z/k_p is denoted as the red curve, while the imaginary part is denoted as the black curve. The IFCs at point C are plotted for (b) TE polarized light and (c) TM polarized light, calculated from the multilayer stack (red-solid curves for the real part and black-solid curves for the imaginary part), the generalized nonlocal EMT (orange-dashed curves for the real part and blue-dashed curves for the imaginary part), and the local EMT (red-dashed curves for the real part and black-dashed curves for the imaginary part).

propagation of the electromagnetic wave in the nonlocal effective medium can be described by the dispersion relation

$$\frac{k_x^2}{\varepsilon_y \mu_z} + \frac{k_z^2}{\varepsilon_y \mu_x} = k_0^2 \tag{11}$$

for the TE polarized light, and

$$\frac{k_x^2}{\varepsilon_z \mu_y} + \frac{k_z^2}{\varepsilon_x \mu_y} = k_0^2 \tag{12}$$

for the TM polarized light. Therefore, according to equations (5), (6), and (9)–(12), the nonlocal effective permittivity and permeability components for the unit cell can be expressed as

$$\begin{cases} \mu_x = \dfrac{k_z/k_0}{\eta_e} \\ \varepsilon_y = \dfrac{k_z}{k_0}\eta_e + \dfrac{k_x^2/k_0^2}{\mu_z} \\ \mu_z \equiv \mu_z^{\mathrm{loc}} = 1 \end{cases} \tag{13}$$

associated with the TE polarized light, while

$$\begin{cases} \varepsilon_x = \dfrac{k_z/k_0}{\eta_e} \\ \mu_y = \dfrac{k_z}{k_0}\eta_e + \dfrac{k_x^2/k_0^2}{\varepsilon_z} \\ \varepsilon_z \equiv \varepsilon_z^{\mathrm{loc}} \end{cases} \tag{14}$$

associated with the TM polarized light. It is noted that three nonlocal effective parameters (μ_x, ε_y, μ_z) or (ε_x, μ_y, ε_z) need to be solved with only two equations of equations (9) and (11) or equations (10) and (12), for TE or TM polarized light. Therefore, the values of the nonlocal effective parameters along the z direction, which is normal to the interfaces of the multilayer stack, are approximated as the values of the corresponding local effective parameters $\mu_z \equiv \mu_z^{\mathrm{loc}}$ and $\varepsilon_z \equiv \varepsilon_z^{\mathrm{loc}}$ in equations (13) and (14). This hypothesis will not reduce the accuracy of the generalized nonlocal EMT due to the relatively weak optical nonlocality along the z direction. Furthermore, based on equation (5), the wave vector k_z in

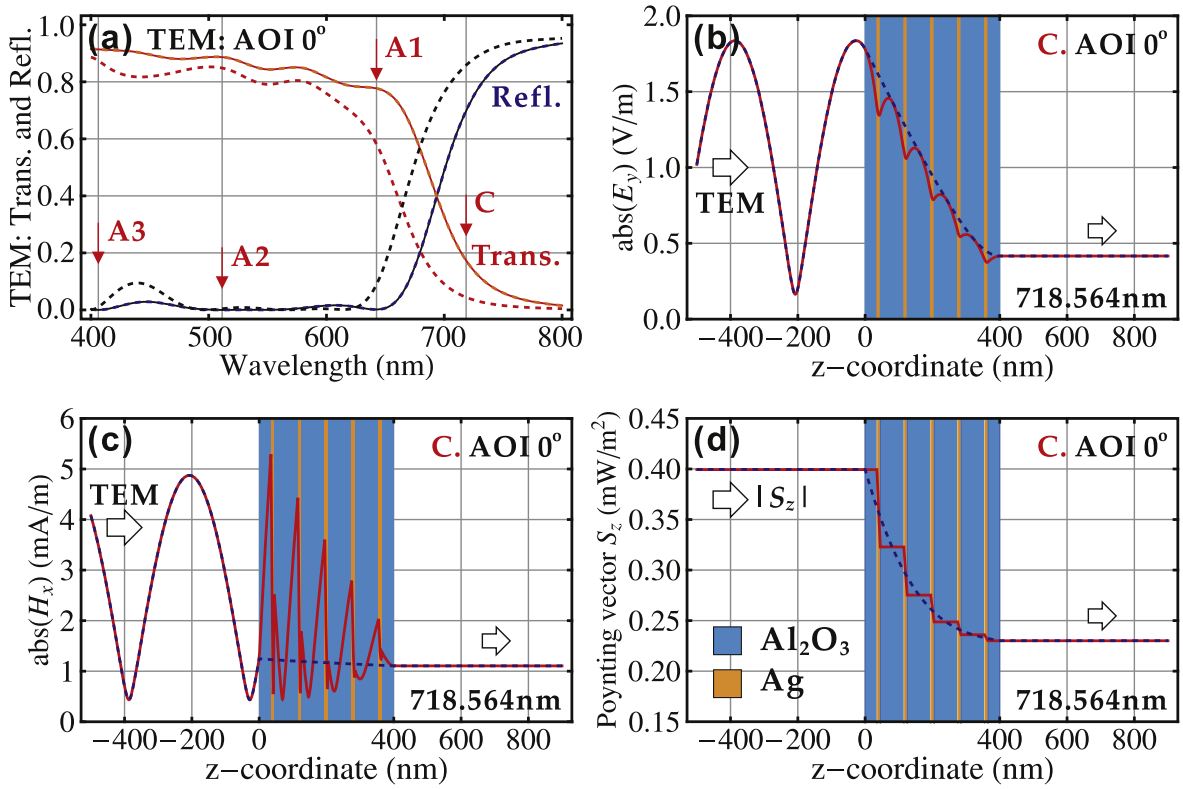

Figure 6. (a) The transmission spectra for the $a = 80$ nm Ag-Al_2O_3 multilayer stack (red-solid curve), the generalized nonlocal EMT (orange-dashed curve), and the local EMT (red-dashed curve), as well as the reflection spectra for the multilayer stack (black-solid curve), the generalized nonlocal EMT (blue-dashed curve), and the local EMT (black-dashed curve) for the TEM mode at zero AOI. The distributions of (b) electric field E_y, (c) magnetic field H_x, and (d) energy flow S_z at point C for the multilayer stack (red-solid curves) and the generalized nonlocal EMT (blue-dashed curves) are displayed.

equations (13) and (14) can be expressed as

$$k_z = \frac{2n\pi \pm \arccos\left[\cos\varphi_d \cos\varphi_m - \frac{1}{2}\left(\frac{\eta_d}{\eta_m} + \frac{\eta_m}{\eta_d}\right)\sin\varphi_d \sin\varphi_m\right]}{a}, \qquad (15)$$

with an arbitrary integer n, which is related to different branches of the real part of wave vector $\mathrm{Re}(k_z)$ and the restriction for the imaginary part of wave vector $\mathrm{Im}(k_z) \geqslant 0$ due to the passive absorption loss. In general, selection of the integer n must lead to a set of nonlocal effective parameters that can converge to the local effective parameters when the period of multilayer stack becomes much less than the wavelength. Moreover, the nonlocal effective parameters must vary continuously with respect to the wavelength or frequency. Additionally, besides the value of the integer n, the plus/minus ($\pm$) sign in equation (15) needs to be properly selected to guarantee the restriction of $\mathrm{Im}(k_z) \geqslant 0$ according to the passive medium condition.

3. Analysis of nonlocal effective permittivity and permeability

The generalized nonlocal EMT will be utilized to study a metal–dielectric multilayer stack in the subwavelength range with the Ag layer thickness of $a_m = 10$ nm and the Al_2O_3 layer thickness of $a_d = 70$ nm in the wavelength range from 400 to 800 nm. The permittivities of the Ag layer and the Al_2O_3 layer, ε_m and ε_d, are obtained from the experimentally measured data [33, 34]. For convenience, the Ag plasma frequency $\omega_p = 1.37 \times 10^{16}\,\mathrm{rad\cdot s^{-1}}$ and the corresponding wave vector $k_p = \omega_p/c$ are applied as the normalization factor in the analysis. According to equation (13), figures 2(a) and (b) display the difference between the nonlocal effective permittivity component ε_y and the local effective permittivity component $\varepsilon_y^{\mathrm{loc}}$, defined as $\Delta\varepsilon_y = \varepsilon_y - \varepsilon_y^{\mathrm{loc}}$, with respect to the variations of wavelength and AOI for TE polarized light. While the difference between the nonlocal effective permeability component μ_x and the local effective permeability component μ_x^{loc}, defined as $\Delta\mu_x = \mu_x - \mu_x^{\mathrm{loc}}$, are shown in figures 2(c) and (d). Similarly, the differences of $\Delta\varepsilon_x = \varepsilon_x - \varepsilon_x^{\mathrm{loc}}$ and $\Delta\mu_y = \mu_y - \mu_y^{\mathrm{loc}}$ for TM polarized light are plotted in figure 3 based on equation (14). The results clearly show that the nonlocal effective permittivity components ε_x and ε_y and the nonlocal effective permeability components μ_x and μ_y are all dependent on both the frequency and the wave vector ($k_x = k_0 \sin\theta_0$) due to the optical nonlocality. In contrast to the local EMT with $\varepsilon_x^{\mathrm{loc}} = \varepsilon_y^{\mathrm{loc}}$ and $\mu_x^{\mathrm{loc}} = \mu_y^{\mathrm{loc}}$, the nonlocal effective parameters $\varepsilon_x \neq \varepsilon_y$ and $\mu_x \neq \mu_y$ when the AOI is not equal to zero. For zero AOI, the TE and TM modes degenerates into the transverse electromagnetic (TEM) mode and thus equation (13) is identical to equation (14).

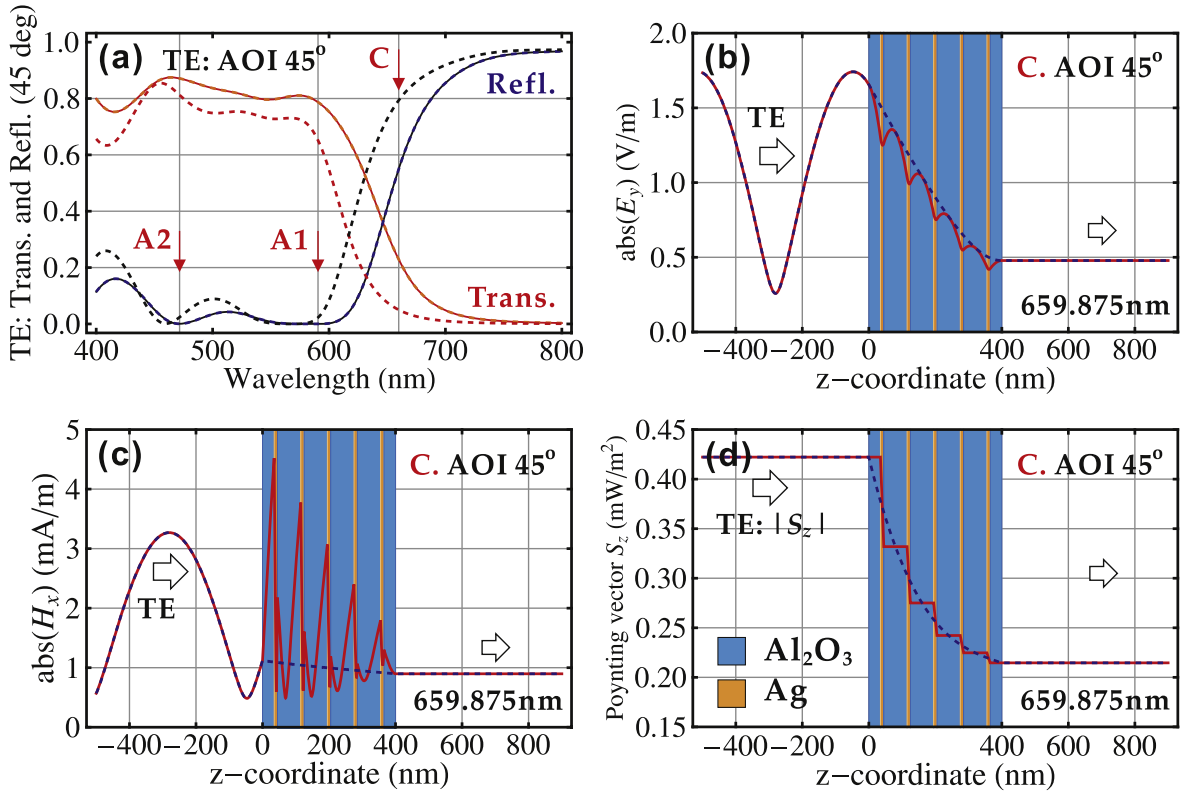

Figure 7. (a) The transmission spectra for the $a = 80$ nm Ag-Al_2O_3 multilayer stack (red-solid curve), the generalized nonlocal EMT (orange-dashed curve), and the local EMT (red-dashed curve), as well as the reflection spectra for the multilayer stack (black-solid curve), the generalized nonlocal EMT (blue-dashed curve), and the local EMT (black-dashed curve) for the TE mode at 45° AOI. The distributions of (b) electric field E_y, (c) magnetic field H_x, and (d) energy flow S_z at point C for the multilayer stack (red-solid curves) and the generalized nonlocal EMT (blue-dashed curves) are displayed.

Moreover, it is noted that the imaginary parts of the nonlocal effective permeability components μ_x and μ_y have negative values. However, this fact does not contradict the passive medium condition, since the imaginary part of the wave vector k_z is always kept as positive value. In addition, it is shown that the nonlocal effective permeability components μ_x and μ_y are sensitive to the configuration of the symmetric unit cell in the metal–dielectric multilayer stack. For the current configuration of the unit cell containing Al_2O_3-Ag-Al_2O_3 structure with the layer thickness of $\frac{1}{2}a_d$-a_m-$\frac{1}{2}a_d$, the nonlocal effective permeability components μ_x and μ_y have values larger than unity, resulting in a paramagnetic response. On the other hand, when the unit cell is switched into Ag-Al_2O_3-Ag structure with the layer thickness of $\frac{1}{2}a_m$-a_d-$\frac{1}{2}a_m$, the nonlocal effective permeability components μ_x and μ_y will have values less than unity, giving a diamagnetic response. Unlike the local EMT and the previous nonlocal EMT, the generalized nonlocal EMT can predict different paramagnetic and diamagnetic responses depending on the unit cell configuration in the metal–dielectric multilayer stack. Since the optical nonlocality is induced by the variation of the electromagnetic field across the scale of the unit cell in the multilayer stack, the nonlocal effective parameters will depend on the period of the unit cell. Figure 4 shows the variations of $\Delta\varepsilon_y$ and $\Delta\mu_x$ with respect to the wavelength and the period of the unit cell for the TEM mode based on equation (13). It is shown that the values of $\Delta\varepsilon_y$ and $\Delta\mu_x$ gradually reduce to zero over the whole wavelength range from 400 to 800 nm as the period of the unit cell reduces from 100 to 10 nm. This means that the optical nonlocal effects are diminished and the nonlocal EMT approaches the local EMT when the size of the unit cell goes to the deep-subwavelength range.

Figure 5(a) plots the band structure of the multilayer stack with the period of the unit cell $a = 80$ nm, according to the diagonalization of the transfer matrix in equation (1) at zero AOI. Four special points are marked in the band structure as point C where $\mathrm{Re}(k_z/k_p) = \mathrm{Im}(k_z/k_p)$, and points A1, A2 and A3 where the Bragg condition is satisfied. At the frequency of point C (417.211 THz or 718.564 nm), the IFCs calculated from the multilayer stack (equation (5)), the generalized nonlocal EMT, and the local EMT are displayed for the TE mode in figure 5(b) and the TM mode in figure 5(c). It is clearly shown that for both TE and TM modes, the IFCs based on the multilayer stack and the generalized nonlocal EMT exactly overlap with each other in both the real part and the imaginary part, implying that the propagation of electromagnetic wave in the multilayer stack can be well described by the generalized nonlocal EMT. In contrast, the IFCs calculated from the local EMT possess a large deviation without the consideration of optical nonlocality. Correspondingly, figure 6 presents the transmission and reflection spectra for the TEM mode with respect to the multilayer stack, the

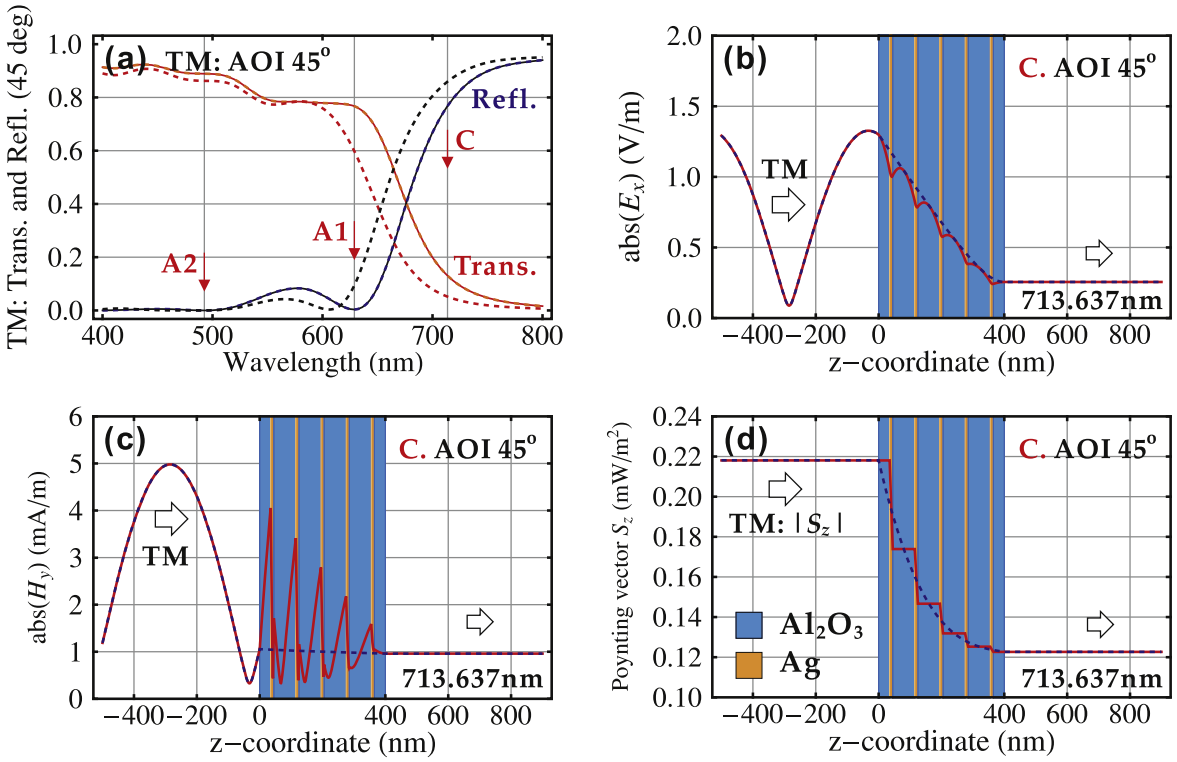

Figure 8. (a) The transmission spectra for the $a = 80$ nm Ag-Al_2O_3 multilayer stack (red-solid curve), the generalized nonlocal EMT (orange-dashed curve), and the local EMT (red-dashed curve), as well as the reflection spectra for the multilayer stack (black-solid curve), the generalized nonlocal EMT (blue-dashed curve), and the local EMT (black-dashed curve) for the TM mode at 45° AOI. The distributions of (b) electric field E_x, (c) magnetic field H_y, and (d) energy flow S_z at point C for the multilayer stack (red-solid curves) and the generalized nonlocal EMT (blue-dashed curves) are displayed.

generalized nonlocal EMT, and the local EMT, together with the distributions of electromagnetic field and energy flow for the multilayer stack and the nonlocal effective medium. The transmission and reflection spectra in figure 6(a) clearly indicate that the generalized nonlocal EMT can predict the exactly same spectra as the multilayer stack, in contrast to the local EMT. The generalized nonlocal EMT also accurately identifies the resonance features at the Bragg condition points (A1, A2 and A3) in the spectra. At the frequency of point C, the distributions of electric field E_y (figure 6(b)) and magnetic field H_x (figure 6(c)) are illustrated for both the multilayer stack and the generalized nonlocal EMT. The electromagnetic field oscillates periodically and decays across each unit cell in the actual multilayer stack, while the electromagnetic field calculated from the generalized nonlocal EMT just smoothly decays through the effective medium without seeing the multilayer interfaces, following the same trend as the multilayer stack. The distribution of energy flow (Poynting vector S_z) along the propagation direction is also plotted in figure 6(d). The energy flow in the multilayer stack has a ladder-like distribution with constant values in Al_2O_3 layers but exponentially decayed values in Ag layers. Instead, the energy flow just exponentially decays along the effective medium based on the generalized nonlocal EMT, with the same trend as the multilayer stack. Moreover, the distributions of electromagnetic field in free space are exactly the same for the multilayer stack and the generalized nonlocal EMT, which indicates the agreement in the calculated transmission and reflection spectra based on both approaches.

Additionally, the generalized nonlocal EMT can also represent the electromagnetic properties of the multilayer stack with respect to the oblique incident light. For instance, figures 7 and 8 display the transmission and reflection spectra related to the multilayer stack, the generalized nonlocal EMT, and the local EMT, together with the distributions of electromagnetic field and energy flow for the multilayer stack and the nonlocal effective medium, with respect to the TE polarized and TM polarized incident light at the AOI of $\theta_0 = 45°$, respectively. Figure 7(a) and 8(a) shows that the generalized nonlocal EMT can still predict the exactly same transmission and reflection spectra as the multilayer stack for both TE mode and TM mode with the oblique incident light, as well as the resonance features at the Bragg condition points (A1 and A2) in contrast to the local EMT. Meanwhile, according to the distributions of electric field E_y (figure 7(b) for TE mode) and E_x (figure 8(b) for TM mode), and magnetic field H_x (figure 7(c) for TE mode) and H_y (figure 8(c) for TM mode) at the frequency of point C, it is shown that the electromagnetic field oscillating and decaying across the multilayer stack is well represented by the generalized nonlocal EMT with smooth decay through the effective medium. Correspondingly, the distributions of energy flow (Poynting vector S_z) with ladder-like profiles in the multilayer stack are also matched well with the results from the generalized

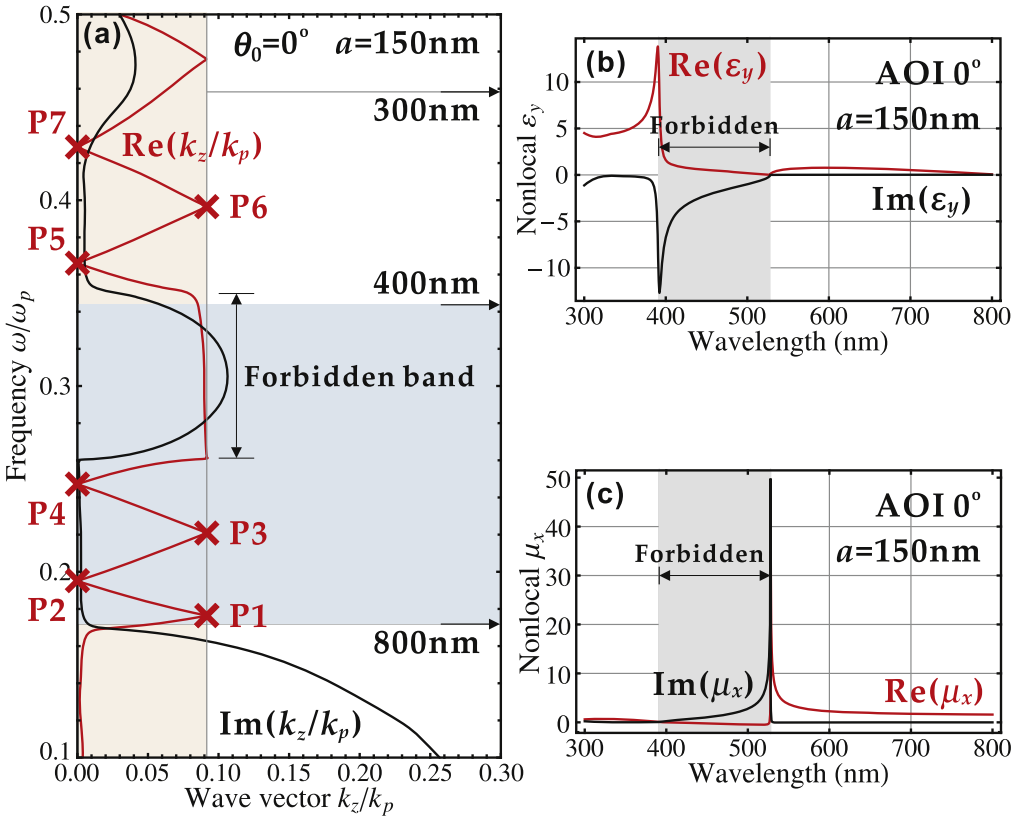

Figure 9. (a) The band structure of the Ag-Al_2O_3 multilayer stack with the period of unit cell $a = 150$ nm at zero AOI. (b) The nonlocal effective permittivity ε_y and (c) the nonlocal effective permeability μ_x with the real part in red-solid curves and the imaginary part in black-solid curves.

nonlocal EMT across the effective medium, as shown in figures 7(d) and 8(d) for the TE mode and TM mode, respectively. Additionally, the distributions of electromagnetic field in free space also agree well between the multilayer stack and the generalized nonlocal EMT for both TE mode and TM mode with the oblique incident light.

Besides the multilayer stack with subwavelength period of the unit cell, the generalized nonlocal EMT can also be utilized to study the case with wavelength-scale period of the unit cell. Figure 9 provides the band structure of the multilayer stack with the period of the unit cell $a = 150$ nm at zero AOI, together with the nonlocal effective parameters over the wavelength range from 300 to 800 nm. Due to the large size of the period, a forbidden band emerges in the band structure approximately from 400 to 520 nm as shown in figure 9(a), leading to strong resonances in the nonlocal effective permittivity ε_y (figure 9(b)) and the nonlocal effective permeability μ_x (figure 9(c)) at the boundaries of the forbidden band due to the band transition. Such band transition induced nonlocal effective parameter resonances can be explained via the branch variation of $\mathrm{Re}(k_z)$ according to equation (15). In general, $\mathrm{Re}(k_z)$ is determined by the $n = 0$ branch with the plus sign in equation (15) in the lower conduction band, but it is determined by the $n = 1$ branch with the minus sign in the forbidden band and upper conduction band. The restriction of $\mathrm{Im}(k_z) \geqslant 0$ should always be guaranteed in all branches to satisfy the passive medium condition. Moreover, the points that satisfy the Bragg condition are all marked in the band structure, with P1 to P4 in the lower conduction band and P5 to P7 in the upper conduction band. The corresponding transmission and reflection spectra, as well as the distributions of electric field are further presented in figure 10. As shown in figure 10(a), the generalized nonlocal EMT can precisely predict the transmission and reflection spectra for the multilayer stack over the whole wavelength range, while the spectra from the local EMT have great deviations since the period of the unit cell is far away from the subwavelength range. Meanwhile, due to the wavelength-scale period of the unit cell, the resonance peaks in the transmission and reflection spectra at the Bragg condition points (P1-P6) are clearly shown. The distributions of electric field E_y at points P1, P3 and P6 are also displayed in figures 10(b)–(d) for both multilayer stack and the generalized nonlocal EMT. Apparently, the electric field in the actual multilayer stack oscillates periodically through each unit cell and generates resonant modes with different orders. While the electric field calculated from the generalized nonlocal EMT exhibits resonant standing wave pattern that matches the electric field of the multilayer stack. These results imply that the generalized nonlocal EMT can well describe the electromagnetic properties for the multilayer stack even in the wavelength-scale range. Meanwhile, the distributions of electric field in free space are exact the same for the multilayer stack and the generalized nonlocal EMT.

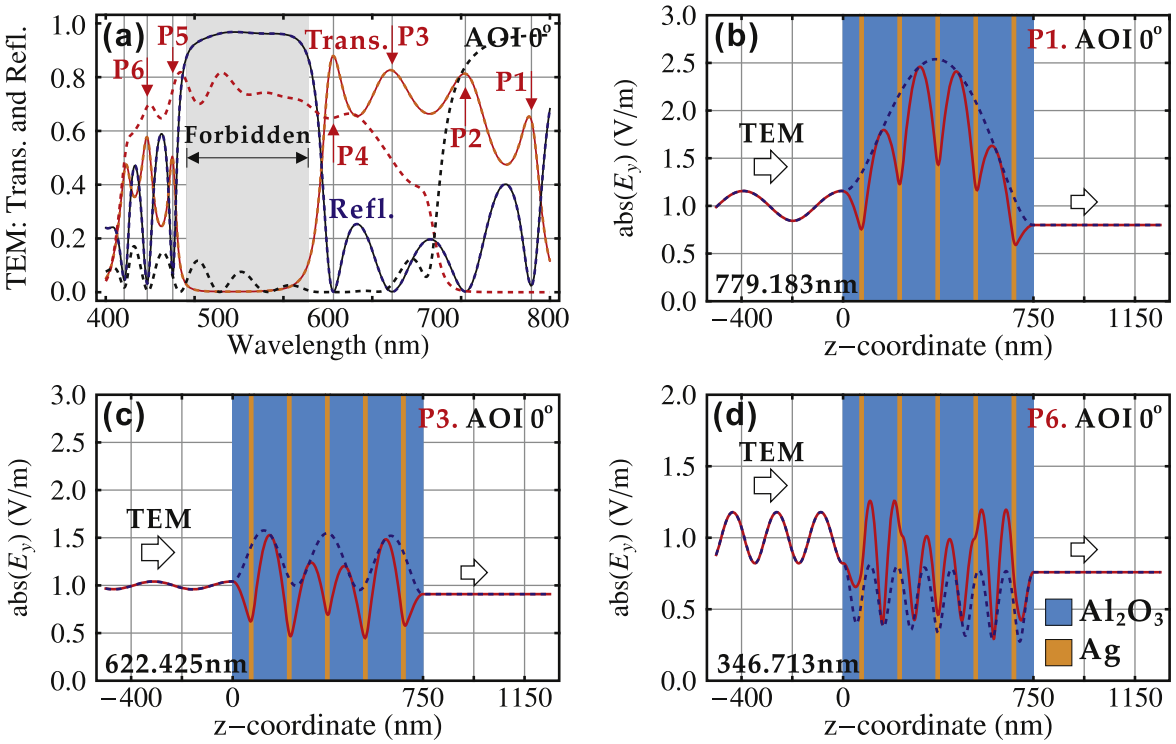

Figure 10. (a) The transmission and reflection spectra for the $a = 150$ nm Ag-Al_2O_3 multilayer stack, the generalized nonlocal EMT, and the local EMT for the TEM mode at zero AOI. The distributions of electric field E_y at (b) point P1, (c) point P3, and (d) point P6 for the multilayer stack (red-solid curves) and the generalized nonlocal EMT (blue-dashed curves) are displayed.

4. Conclusions

A generalized nonlocal EMT in consideration of nonlocal effective permittivity and permeability has been derived through the transfer-matrix method for symmetric and periodic metal–dielectric multilayer stacks, with respect to both TE and TM polarized light with arbitrary angle of incidence. The nonlocal effective permittivity and permeability tensors depending on both frequency and wave vector have been analyzed in detail as functions of the wavelength, the angle of incidence, and the period of the unit cell. The generalized nonlocal EMT will converge into the local EMT as the period of the unit cell approaches zero. In contrast to the local EMT, the generalized nonlocal EMT can accurately characterize the band structures, IFCs, transmission and reflection spectra, and optical field distributions for the symmetric metal–dielectric multilayer stacks with either subwavelength or wavelength-scale period of the unit cell.

Acknowledgments

The authors acknowledge support from the National Science Foundation under Grant No. DMR-1552871 and CBET-1402743, and U.S. Army Research Office Award No. W911NF-15-1-0477.

References

[1] Poddubny A, Iorsh I, Belov P and Kivshar Y 2013 Hyperbolic metamaterials *Nat. Photonics* **7** 958–67
[2] Chui S T, Chan C T and Lin Z F 2006 Multilayer structures as negative refractive and left-handed materials *J. Phys.: Condens. Matter* **18** L89–95
[3] Hoffman A J, Alekseyev L, Howard S S, Franz K J, Wasserman D, Podolskiy V A, Narimanov E E, Sivco D L and Gmachl C 2007 Negative refraction in semiconductor metamaterials *Nat. Mater.* **6** 946–50
[4] Zhao J, Gao J, Deng Y, Liu H and Wang X 2014 Negative refraction by a planar Ag/SiO_2 multilayer at ultraviolet wavelength to the limit of silver *AIP Adv.* **4** 047127
[5] Jacob Z, Alekseyev L V and Narimanov E 2006 Optical hyperlens: far-field imaging beyond the diffraction limit *Opt. Express* **14** 8247–56
[6] Liu Z, Lee H, Xiong Y, Sun C and Zhang X 2007 Far-field optical hyperlens magnifying sub-diffraction-limited objects *Science* **315** 1686
[7] Zhang X and Liu Z 2008 Superlenses to overcome the diffraction limit *Nat. Mater.* **7** 435–41
[8] Yang X, Yao J, Rho J, Yin X and Zhang X 2012 Experimental realization of three-dimensional indefinite cavities at the nanoscale with anomalous scaling laws *Nat. Photonics* **6** 450–4
[9] Noginov M A, Li H, Barnakov Y A, Dryden D, Nataraj G, Zhu G, Bonner C E, Mayy M, Jacob Z and Narimanov E E 2010 Controlling spontaneous emission with metamaterials *Opt. Lett.* **35** 1863–5
[10] Jacob Z, Kim J, Naik G, Boltasseva A, Narimanov E and Shalaev V 2010 Engineering photonic density of states using metamaterials *Appl. Phys.* B **100** 215–8

[11] Guo Y, Cortes C L, Molesky S and Jacob Z 2012 Broadband super-Planckian thermal emission from hyperbolic metamaterials *Appl. Phys. Lett.* **101** 131106
[12] Jacob Z, Smolyaninov I I and Narimanov E E 2012 Broadband Purcell effect: radiative decay engineering with metamaterials *Appl. Phys. Lett.* **100** 181105
[13] Iorsh I, Poddubny A, Orlov A, Belov P and Kivshar Y S 2012 Spontaneous emission enhancement in metal–dielectric metamaterials *Phys. Lett.* A **376** 185–7
[14] Lu D, Kan J J, Fullerton E E and Liu Z 2014 Enhancing spontaneous emission rates of molecules using nanopatterned multilayer hyperbolic metamaterials *Nat. Nanotechnol.* **9** 48–53
[15] Alù A, Silveirinha M G, Salandrino A and Engheta N 2007 Epsilon-near-zero metamaterials and electromagnetic sources: tailoring the radiation phase pattern *Phys. Rev.* B **75** 155410
[16] Engheta N 2007 Circuits with light at nanoscales: optical nanocircuits inspired by metamaterials *Science* **317** 1698–702
[17] Silveirinha M and Engheta N 2009 Transporting an image through a subwavelength hole *Phys. Rev. Lett.* **102** 103902
[18] Argyropoulos C, Chen P, D'Aguanno G, Engheta N and Alù A 2012 Boosting optical nonlinearities in ε-near-zero plasmonic channels *Phys. Rev.* B **85** 045129
[19] Alù A and Engheta N 2005 Achieving transparency with plasmonic and metamaterial coatings *Phys. Rev.* E **72** 016623
[20] Pendry J B, Schurig D and Smith D R 2006 Controlling electromagnetic fields *Science* **312** 1780–2
[21] Elser J, Podolskiy V A, Salakhutdinov I and Avrutsky I 2007 Nonlocal effects in effective-medium response of nanolayered metamaterials *Appl. Phys. Lett.* **90** 191109
[22] Sun L, Gao J and Yang X 2013 Giant optical nonlocality near the Dirac point in metal–dielectric multilayer metamaterials *Opt. Express.* **21** 21542–55
[23] Gao J, Sun L, Deng H, Mathai C J, Gangopadhyay S and Yang X 2013 Experimental realization of epsilon-near-zero metamaterial stacks with metal–dielectric multilayers *Appl. Phys. Lett.* **103** 051111
[24] Sun L, Cheng F, Mathai C J, Gangopadhyay S, Gao J and Yang X 2014 Experimental characterization of optical nonlocality in metal–dielectric multilayer metamaterials *Opt. Express* **22** 22974–80
[25] Chebykin A V, Orlov A A, Vozianova A V, Maslovski S I, Kivshar Yu S and Belov P A 2011 Nonlocal effective medium model for multilayered metal–dielectric metamaterials *Phys. Rev.* B **84** 115438
[26] Chebykin A V, Orlov A A, Simovski C R, Kivshar Y S and Belov P A 2012 Nonlocal effective parameters of multilayered metal–dielectric metamaterials *Phys. Rev.* B **86** 115420
[27] Sun L, Li Z, Luk T S, Yang X and Gao J 2015 Nonlocal effective medium analysis in symmetric metal–dielectric multilayer metamaterials *Phys. Rev.* B **91** 195147
[28] Herpin A 1947 Optique Électromagnétique-calcul du pouvior réflecteur dun systeme stratifie quelconque *Compt. Rend.* **225** 182–3
[29] Epstein L I 1952 The design of optical filters *J. Opt. Soc. Am.* **42** 806–8
[30] Thelen A 1966 Equivalent layers in multilayer filters *J. Opt. Soc. Am.* **56** 1533–8
[31] Young P A 1970 Extension of Herpin's theorem *J. Opt. Soc. Am.* **60** 1422–3
[32] Born M and Wolf E 1999 *Principles of Optics: Electromagnetic Theory of Propagation, Interference and Diffraction of Light* (Cambridge, UK: Cambridge University Press)
[33] Johnson P B and Christy R W 1972 Optical constant of the noble metals *Phys. Rev.* B **6** 4370–9
[34] Malitson I H 1962 Refraction and dispersion of synthetic sapphire *J. Opt. Soc. Am.* **52** 1377–9